

**A search for a dark matter annihilation signal
towards the Canis Major overdensity with H.E.S.S.**

F. Aharonian^{1,13}, A.G. Akhperjanian², U. Barres de Almeida^{8,*}, A.R. Bazer-Bachi³, B. Behera¹⁴,
W. Benbow¹, K. Bernlöhr^{1,5}, C. Boisson⁶, V. Bochow¹, V. Borrel³, I. Braun¹, E. Brion⁷,
J. Brucker¹⁶, P. Brun⁷, R. Bühler¹, T. Bulik²⁴, I. Büsching⁹, T. Boutelier¹⁷, S. Carrigan¹,
P.M. Chadwick⁸, A. Charbonnier¹⁹, R.C.G. Chaves¹, A. Cheesebrough⁸, L.-M. Chounet¹⁰,
A.C. Clapson¹, G. Coignet¹¹, L. Costamante^{1,29}, M. Dalton⁵, B. Degrange¹⁰, C. Deil¹,
H.J. Dickinson⁸, A. Djannati-Ataï¹², W. Domainko¹, L.O'C. Drury¹³, F. Dubois¹¹, G. Dubus¹⁷,
J. Dyks²⁴, M. Dyrda²⁸, K. Egberts¹, D. Emmanoulopoulos¹⁴, P. Espigat¹², C. Farnier¹⁵,
F. Feinstein¹⁵, A. Fiasson¹⁵, A. Förster¹, G. Fontaine¹⁰, M. Füßling⁵, S. Gabici¹³, Y.A. Gallant¹⁵,
L. Gérard¹², B. Giebels¹⁰, J.F. Glicenstein⁷, B. Glück¹⁶, P. Goret⁷, C. Hadjichristidis⁸,
D. Hauser¹, M. Hauser¹⁴, S. Heinz¹⁶, G. Heinzelmann⁴, G. Henri¹⁷, G. Hermann¹, J.A. Hinton²⁵,
A. Hoffmann¹⁸, W. Hofmann¹, M. Holleran⁹, S. Hoppe¹, D. Horns¹⁸, A. Jacholkowska¹⁵,
O.C. de Jager⁹, I. Jung¹⁶, K. Katarzyński²⁷, S. Kaufmann¹⁴, E. Kendziorra¹⁸, M. Kerschhaggl⁵,
D. Khangulyan¹, B. Khélifi¹⁰, D. Keogh⁸, Nu. Komin¹⁵, K. Kosack¹, G. Lamanna¹¹,
J.-P. Lenain⁶, T. Lohse⁵, V. Marandon¹², J.M. Martin⁶, O. Martineau-Huynh¹⁹, A. Marcowith¹⁵,
D. Maurin¹⁹, T.J.L. McComb⁸, C. Medina⁶, R. Moderski²⁴, E. Moulin⁷, M. Naumann-Godo¹⁰,
M. de Naurois¹⁹, D. Nedbal²⁰, D. Nekrassov¹, J. Niemiec²⁸, S.J. Nolan⁸, S. Ohm¹, J-F. Olive³,
E. de Oña Wilhelmi¹², K.J. Orford⁸, J.L. Osborne⁸, M. Ostrowski²³, M. Panter¹, G. Pedalletti¹⁴,
G. Pelletier¹⁷, P.-O. Petrucci¹⁷, S. Pita¹², G. Pühlhofer¹⁴, M. Punch¹², A. Quirrenbach¹⁴,
B.C. Raubenheimer⁹, M. Raue⁴, S.M. Rayner⁸, M. Renaud¹, F. Rieger^{1,29}, J. Ripken⁴, L. Rob²⁰,
S. Rosier-Lees¹¹, G. Rowell²⁶, B. Rudak²⁴, C.B. Rulten⁸, J. Ruppel²¹, V. Sahakian²,
A. Santangelo¹⁸, R. Schlickeiser²¹, F.M. Schöck¹⁶, R. Schröder²¹, U. Schwanke⁵, S. Schwarzburg¹⁸,
S. Schwemmer¹⁴, A. Shalchi²¹, J.L. Skilton²⁵, H. Sol⁶, D. Spangler⁸, L. Stawarz²³,
R. Steenkamp²², C. Stegmann¹⁶, G. Superina¹⁰, P.H. Tam¹⁴, J.-P. Tavernet¹⁹, R. Terrier¹²,
O. Tibolla¹⁴, C. van Eldik¹, G. Vasileiadis¹⁵, C. Venter⁹, J.P. Vialle¹¹, P. Vincent¹⁹, M. Vivier^{7,†},
H.J. Völk¹, F. Volpe^{10,29}, S.J. Wagner¹⁴, M. Ward⁸, A.A. Zdziarski²⁴, A. Zech⁶

-
- ¹Max-Planck-Institut für Kernphysik, P.O. Box 103980, D 69029 Heidelberg, Germany
- ²Yerevan Physics Institute, 2 Alikhanian Brothers St., 375036 Yerevan, Armenia
- ³Centre d'Etude Spatiale des Rayonnements, CNRS/UPS, 9 av. du Colonel Roche, BP 4346, F-31029 Toulouse Cedex 4, France
- ⁴Universität Hamburg, Institut für Experimentalphysik, Luruper Chaussee 149, D 22761 Hamburg, Germany
- ⁵Institut für Physik, Humboldt-Universität zu Berlin, Newtonstr. 15, D 12489 Berlin, Germany
- ⁶LUTH, Observatoire de Paris, CNRS, Université Paris Diderot, 5 Place Jules Janssen, 92190 Meudon, France
- ⁷IRFU/DSM/CEA, CE Saclay, F-91191 Gif-sur-Yvette, Cedex, France
- ⁸University of Durham, Department of Physics, South Road, Durham DH1 3LE, U.K.
- ⁹Unit for Space Physics, North-West University, Potchefstroom 2520, South Africa
- ¹⁰Laboratoire Leprince-Ringuet, Ecole Polytechnique, CNRS/IN2P3, F-91128 Palaiseau, France
- ¹¹Laboratoire d'Annecy-le-Vieux de Physique des Particules, CNRS/IN2P3, 9 Chemin de Bellevue - BP 110 F-74941 Annecy-le-Vieux Cedex, France
- ¹²Astroparticule et Cosmologie (APC), CNRS, Université Paris 7 Denis Diderot, 10, rue Alice Domon et Leonie Duquet, F-75205 Paris Cedex 13, France
Also at UMR 7164 (CNRS, Université Paris VII, CEA, Observatoire de Paris)
- ¹³Dublin Institute for Advanced Studies, 5 Merrion Square, Dublin 2, Ireland
- ¹⁴Landessternwarte, Universität Heidelberg, Königstuhl, D 69117 Heidelberg, Germany
- ¹⁵Laboratoire de Physique Théorique et Astroparticules, CNRS/IN2P3, Université Montpellier II, CC 70, Place Eugène Bataillon, F-34095 Montpellier Cedex 5, France
- ¹⁶Universität Erlangen-Nürnberg, Physikalisches Institut, Erwin-Rommel-Str. 1, D 91058 Erlangen, Germany
- ¹⁷Laboratoire d'Astrophysique de Grenoble, INSU/CNRS, Université Joseph Fourier, BP 53, F-38041 Grenoble Cedex 9, France
- ¹⁸Institut für Astronomie und Astrophysik, Universität Tübingen, Sand 1, D 72076 Tübingen, Germany
- ¹⁹LPNHE, Université Pierre et Marie Curie Paris 6, Université Denis Diderot Paris 7, CNRS/IN2P3, 4 Place Jussieu, F-75252, Paris Cedex 5, France
- ²⁰Institute of Particle and Nuclear Physics, Charles University, V Holesovickach 2, 180 00 Prague 8, Czech Republic
- ²¹Institut für Theoretische Physik, Lehrstuhl IV: Weltraum und Astrophysik, Ruhr-Universität Bochum, D 44780 Bochum, Germany
- ²²University of Namibia, Private Bag 13301, Windhoek, Namibia
- ²³Obserwatorium Astronomiczne, Uniwersytet Jagielloński, Kraków, Poland
- ²⁴Nicolaus Copernicus Astronomical Center, Warsaw, Poland
- ²⁵School of Physics & Astronomy, University of Leeds, Leeds LS2 9JT, UK
- ²⁶School of Chemistry & Physics, University of Adelaide, Adelaide 5005, Australia
- ²⁷Toruń Centre for Astronomy, Nicolaus Copernicus University, Toruń, Poland
- ²⁸Instytut Fizyki Jadrowej PAN, ul. Radzikowskiego 152, 31-342 Kraków, Poland

Abstract

A search for a dark matter (DM) annihilation signal into γ -rays toward the direction of the Canis Major (CMa) overdensity is presented. The nature of CMa is still controversial and one scenario represents it as a dwarf galaxy, making it an interesting candidate for DM annihilation searches. A total of 9.6 hours of high quality data were collected with the H.E.S.S. array of Imaging Atmospheric Cherenkov Telescopes (IACTs) and no evidence for a very high energy γ -ray signal is found. Upper limits on the CMa dwarf galaxy mass of the order of $10^9 M_\odot$ are derived at the 95% C.L. assuming neutralino masses in the range 500 GeV - 10 TeV and relatively large annihilation cross-sections. Constraints on the velocity-weighted annihilation cross section $\langle\sigma v\rangle$, are calculated for specific WIMP scenarios, using a NFW model for the DM halo profile and taking advantage of numerical simulations of hierarchical structure formation. 95% C.L. exclusion limits of the order of $5 \times 10^{-24} \text{ cm}^3 \text{ s}^{-1}$ are reached in the 500 GeV - 10 TeV DM particle mass interval, assuming a total halo mass of $3 \times 10^8 M_\odot$.

Subject headings: gamma rays - dark matter - galaxies: dwarf

1. Introduction

It is widely believed that around one third of the energy content of the Universe is made of cold matter, of which only a small fraction is luminous and is of baryonic origin. In the framework of the Cold Dark Matter (CDM) scenarios, most of the matter is composed of non-baryonic Weakly Interacting Massive Particles (WIMPs). The standard model of particle physics does not provide a natural and suitable candidate for the Dark Matter (DM) particle and many theories beyond the standard model have been proposed to explain its origin and properties (see (3) for a recent review). In various models, the self-annihilation of WIMPs gives a γ -ray continuum emission resulting from the hadronization of primary annihilation products. The spectral features of such a DM annihilation radiation might help to distinguish it from ordinary astrophysical sources (Bergström et al. 2005a; Bergström et al. 2005b). The indirect detection of DM through very high energy (VHE) γ -rays is one of the best ways to probe the astrophysical nature of the DM and the H.E.S.S. array of Cherenkov telescopes, dedicated for detection of VHE γ -rays in the 100 GeV-10 TeV energy regime, is an interesting instrument for this purpose.

Many astrophysical objects, ranging from DM clumps to galaxy clusters are expected to lead to DM particle annihilation signals detectable with sufficiently sensitive instruments. Regions of high

²⁹European Associated Laboratory for Gamma-Ray Astronomy, jointly supported by CNRS and MPG

*supported by CAPES Foundation, Ministry of Education of Brazil

†matthieu.vivier@cea.fr

concentration of DM are good candidates to search for such annihilations and the Galactic Centre (GC) was first considered. H.E.S.S. observations of the GC region (Aharonian et al. 2004) revealed a source of VHE γ -ray emission (HESS J1745-290) but ruled out the bulk of the signal as of DM origin (Aharonian et al. 2006c). Prospects for indirect detection in the elliptical galaxy M87 at the center of the Virgo cluster were also investigated. The time variability of the VHE γ -ray signal observed by H.E.S.S. (Aharonian et al. 2006a) gave clear evidence that the signal was not of a sole DM origin. There are also other candidates with high DM density in relative proximity that might lead to detectable DM annihilation signals. Satellite dwarf galaxies of the Milky Way (MW) such as Sagittarius, Draco or Canis Major are popular targets, owing to their relatively low astrophysical background (6). Indeed, dwarf spheroidal galaxies usually consist of stellar populations with no hot or warm gas and no cosmic rays, and are among the most extreme DM-dominated environments. A null result concerning the search for DM toward the Sagittarius dwarf spheroidal galaxy (Sgr dSph) direction was published by the H.E.S.S. collaboration (Aharonian et al. 2008). Constraints on the parameter spaces of two popular WIMPs models, namely the R-parity conserving Minimal Supersymmetric extension of the Standard Model (MSSM) and Kaluza-Klein (KK) scenarios with K-parity conservation, were derived. A null result was also established by the MAGIC collaboration (Albert et al. 2007) and the WHIPPLE collaboration (Wood et al. 2007), when searching for a DM annihilation signal toward the Draco dwarf galaxy. Upper limits on the velocity-weighted annihilation cross-section of DM particle were derived in the framework of minimal Super GRAvity (mSUGRA) models and MSSM models, respectively.

The present paper reports the search for a DM annihilation signal towards the direction of the CMa overdensity with the H.E.S.S. array of Cherenkov telescopes. The paper is organized as follows: in Sec. II the controversial nature of the CMa overdensity is briefly discussed; in Sec. III the analysis of the data is presented, while in Sec. IV the predictions for DM annihilation into γ -rays in the CMa overdensity are discussed. Constraints on the WIMP velocity-weighted annihilation rate, as well as on the CMa total mass, are given.

2. A Galactic warp or the relic of a dwarf galaxy?

Since its discovery (Martin et al. 2004), the nature of the Canis Major (CMa) overdensity is the subject of many discussions over whether it is a dwarf galaxy or simply a part of the warped Galactic disk. According to (Momany et al. 2006), the CMa overdensity simply reflects the warp and flare of the outer disk, a structure frequently observed in spiral galaxies such as the MW. The comparison of the kinematics of the CMa stars with those of the Galactic thick disk shows that the CMa stars do not have peculiar proper motions, which cast some doubts on the dwarf Spheroidal (dSph) nature of the CMa overdensity. The second scenario, which is of interest for the aim of this paper, considers this elliptical overdensity as the remnant of a disrupted dwarf galaxy that could have created the Monoceros “ring” structure (Martin et al. 2004). Indeed, numerical simulations show that such a structure can be explained by an in-plane accretion event, in which the remnant of the dwarf galaxy would have an orbital plane close to the Galactic plane. Another argument

in favor of this scenario is that the CMa star populations do not exhibit the same properties as those in the disk since they have a relatively low metallicity (de Jong et al. 2007). In this case, the CMa star population would not belong to the Galactic disk, in contrast to what was found in (Momany et al. 2006). The mass, luminosity and characteristic dimensions of CMa appear quite similar to those of the Sgr dwarf galaxy. As for many dSph, the CMa overdensity would thus be an interesting candidate for DM detection. In the remainder of the paper, the Canis Major object is assumed to be a dwarf galaxy.

The CMa overdensity is located towards the Galactic anti-centre direction at roughly 8 kpc from the sun (Bellazinni et al. 2004) and is the closest observed dwarf galaxy. It is a very extended object ($\Delta l = 12^\circ$, $\Delta b = 10^\circ$) with a roundish core approximately centered at $l = 240^\circ$ and $b = -8^\circ$ according to various star surveys in this region (Martin et al. 2004; Martinez et al. 2004). In contrast to the Sgr dSph, neither dispersion velocity measurements, nor luminosity profiles are available so that an accurate modelling of the CMa DM halo profile is not possible. However, there are enough constraints to estimate the expected γ -ray flux from DM particle annihilations in this object. The annihilation cross-section is given by the particle physics model (see section IV). As concerns the mass content of CMa, the narrow dispersion between the average mass values found for different dSph galaxies in the local group (Mateo 1998; Walker et al. 2007) is an indication that dSph's may possibly have a universal host halo mass (Dekel and Silk 1986). The mass of the CMa dwarf galaxy can then be inferred to be in the same range as the Sgr dwarf galaxy and many other dSph's so that the CMa total mass would range between 10^8 and $10^9 M_\odot$ (Martin et al. 2004). For instance, reference (6) gives a model where the CMa mass is taken as $3 \times 10^8 M_\odot$. The H.E.S.S. large FoV covers a large part of the CMa core, optimizing the chances to see a potential DM annihilation signal.

3. H.E.S.S. observations and analysis

3.1. The H.E.S.S. array of Imaging Atmospheric Cherenkov Telescopes

H.E.S.S. is an array of four Imaging Atmospheric Cherenkov Telescopes (IACT's) (Hofmann et al. 2003) located in the Khomas Highland of Namibia at an altitude of 1800 m above sea level. The instrument uses the atmosphere as a calorimeter and images electromagnetic showers induced by TeV γ -rays. Each telescope collects the Cherenkov light radiated by particle cascades in the air showers using a large mirror area of 107 m^2 and a camera of 960 photomultiplier tubes (PMT's). The four telescopes are placed in a square formation with a side length of 120 m. This configuration allows for a accurate reconstruction of the direction and energy of the γ -rays using the stereoscopic technique. The cameras cover a total field of view of 5° in diameter. The energy threshold of the H.E.S.S. instrument is approximately 100 GeV at zenith and its sensitivity allows to detect fluxes larger than $2 \times 10^{-13} \text{ cm}^{-2} \text{ s}^{-1}$ above 1 TeV in 25 hours. More details on the H.E.S.S. experiment can be found in (Aharonian et al. 2006b).

3.2. Data processing

Observations of the CMa dwarf galaxy with H.E.S.S. were carried out in November 2006 with pointing angles close to the zenith and extending up to 20° . The nominal pointing direction was $l = 240.15^\circ$ and $b = -8.07^\circ$ in Galactic coordinates. The data were taken in “wobble mode” with the telescope pointing typically shifted by $\pm 0.7^\circ$ from the nominal target position (1). The wobble observing mode reduces the systematic effects in the background estimates. The dataset used for image analysis was selected using the standard quality criteria, excluding runs taken under bad or variable weather conditions. The CMa dataset amounts to 9.6 hours of live time after quality selection.

Two different techniques are combined for the data processing. The first technique computes the “Hillas geometrical moments” of the shower images to reconstruct shower geometry and energy, and to discriminate between γ -ray and hadronic events (Aharonian et al. 2005). The second technique uses a semi-analytical model of air showers which predicts the expected intensity in each camera pixel (de Naurois et al. 2003). Here, the shower direction, the impact point and the primary particle energy are derived with a likelihood fit of the shower model to match the images. Standard cuts for γ -ray/hadron separations are derived by simulations. Both analyses provide an energy resolution of 15% and an angular resolution better than 0.1° . The combination of these two techniques, referred hereafter as “Combined Hillas/Model analysis”, uses a combined estimator (the so-called “Combined cut”) and provides an improved background rejection. The background is estimated following the template background method. This method uses events that fail the γ -ray selection cuts. The template background modelling is well suited for the detection of sources positioned anywhere in the FoV, as it estimates the background in each sky direction. More details on this background subtraction method are given in (Rowell 2003). A charge cut of 60 photoelectrons on the image size is applied, as well as a cut on the primary interaction depth of particles to optimize the signal-to-noise ratio. Events that pass the analysis cuts are labelled as “ γ candidates” and are stored in the so-called γ candidate map $n_\gamma^{\text{candidate}}(l, b)$. Events that do not pass the analysis cuts are defined as “background events” and are stored in the so-called background map $n_{\text{bck}}(l, b)$. Table 1 shows the different cut values used to select the γ -ray events. The $2.5^\circ \times 2.5^\circ$ excess sky map is obtained by the following equation:

$$n_\gamma^{\text{excess}}(l, b) = n_\gamma^{\text{candidate}}(l, b) - \alpha(l, b) \times n_{\text{bck}}(l, b), \quad (1)$$

where $\alpha(l, b)$ refers to the template normalisation factor as described in (Rowell 2003). To search for a gamma-ray signal, the raw fine-binned maps are integrated with a 0.1° radius around each point to match the H.E.S.S. angular resolution, resulting in new oversampled maps of gamma-ray candidates and background events, and a corresponding gamma-ray excess map. Using the prescription of Li and Ma (Li and Ma 1983) to derive the significance for each point of the oversampled map on the basis of the gamma-ray candidate and background counts and the template normalization factor, no significant excess is found at the target position or at other points in the field of view (Fig. 1(a)). The distribution of significances for the entire map is shown in Fig. 1(b) and is fully consistent with statistical fluctuations of the background signal. As the excess map does not show

any signal, an upper limit on the number of gamma-ray events for each point in the map can be derived using the method of Feldman and Cousins (Feldman and Cousins 1998). The uncorrelated γ candidate and normalized background maps, plotted on a $0.2^\circ \times 0.2^\circ$ grid to have bins not smaller than the H.E.S.S. angular resolution, are used for the upper limits calculations.

4. Predictions for Dark Matter annihilations in the Canis Major overdensity

The DM particles are expected to annihilate into a continuum of γ -rays through various processes such as the hadronization of quark final states, hadronic decay of τ leptons and subsequent decay of mesons. Two DM candidates are commonly discussed in literature: the so-called neutralino arising in supersymmetric extensions of the standard model (SUSY) (7), and the first excitation of the hypercharge gauge boson in Universal Extra Dimension theories (UED) called the $B^{(1)}$ particle (Servant and Tait 2003). Typical masses for these DM candidates range from 50 GeV to several TeV. The value of the annihilation cross-section is constrained to give a thermal relic abundance of WIMPs that is in agreement with the WMAP+SDSS derived value (Tegmark et al. 2006). The velocity-weighted annihilation cross-sections can be as low as $10^{-30} \text{ cm}^3 \text{ s}^{-1}$, for scenarios involving co-annihilations processes, and be as high as $10^{-25} \text{ cm}^3 \text{ s}^{-1}$.

The expected flux ϕ_γ of γ -rays from WIMP annihilations occurring in a spherical dark halo is commonly written as a product of a particle physics term ($d\Phi^{\text{PP}}/dE_\gamma$) and an astrophysics term (f^{AP}):

$$\phi_\gamma = \frac{d\Phi^{\text{PP}}}{dE_\gamma} \times f^{\text{AP}} \quad (2)$$

The expected number of γ -ray is then given by:

$$N_\gamma = T_{\text{ON}} \times \int_0^{m_{\text{DM}}c^2} \frac{1}{A_{\text{eff}}(E_\gamma)} \phi_\gamma(E_\gamma) dE_\gamma, \quad (3)$$

Cut name	γ -event cut value
Combined cut	≤ 0.7
Image charge min.	≥ 60 photo-electrons
Reconstructed shower depth min.(rad. length)	-1
Reconstructed shower depth max. (rad. length)	4
Reconstructed nominal distance	$\leq 2.5^\circ$
Reconstructed event telescope multiplicity	≥ 2

Table 1: List of cuts used in the analysis. The shower depth is the reconstructed primary interaction depth of the particles. The nominal distance is the angular distance of the image barycenter to the center of the camera.

where T_{ON} denotes the ON-source exposure time, which depends on the pointing direction, and $\overline{A_{\text{eff}}}(E_\gamma)$ the averaged H.E.S.S. acceptance during data collection. The velocity-weighted cross-section for WIMP annihilation $\langle\sigma v\rangle$ and the WIMP mass are fixed to compute the particle physics term in Eq.2:

$$\frac{d\Phi^{\text{PP}}}{dE_\gamma} = \frac{\langle\sigma v\rangle}{4\pi m_{\text{DM}}^2} \left(\frac{dN}{dE_\gamma} \right)_{\text{DM}}, \quad (4)$$

where $(dN/dE_\gamma)_{\text{DM}}$ is the γ -ray spectrum originating for DM particle annihilation. The shape of the continuum γ -ray spectrum predicted in the framework of the phenomenological Minimal Supersymmetric extension of the Standard Model (pMSSM) depends on the model in a complicated way. A simplified parametrization of this shape, for higgsino-like neutralinos mainly annihilating via pairs of W and Z gauge bosons, was taken from (2). In the case of KK $B^{(1)}$ particle annihilations, the branching ratios to final states are independent of the WIMP mass. The differential photon continuum has been simulated with the PYTHIA package (Sjöstrand T. et al. 2003) using branching ratios from (Servant and Tait 2003).

The astrophysics term f^{AP} illustrates the DM concentration dependency of the expected γ -ray flux toward the pointed source:

$$f^{\text{AP}} = \int_{\Delta\Omega} \int_{\text{los}} \rho^2(l) dl d\Omega, \quad (5)$$

where $\rho(l)$ is the mass density profile of the CMa dwarf galaxy and $\Delta\Omega$ the detection solid angle ($\Delta\Omega = 10^{-5}$ sr, corresponding to the integration radius of 0.1°).

4.1. Model of the Canis Major Dark Matter halo within the Λ CDM cosmology

The purpose of this section is to explain how the astrophysical term f^{AP} (Eq. 2, Eq. 5) was calculated as a function of the total CMa dark halo mass. The estimate of the astrophysical term f^{AP} relies on the modelling of the CMa DM mass distribution. Observationally, the DM mass content of dSph galaxies can be derived using velocity dispersion measurements of their stellar population as well as their luminosity profile. The comparison between models and observations can constrain the parameters of their assumed density profiles. In the case of the CMa dSph, the lack of available observational data prevents the modelling of its density profile in the same way as in the literature (6; 4; Aharonian et al. 2008).

In the absence of observational data, a standard cusped NFW halo (8) was assumed to model the CMa dwarf mass distribution:

$$\rho_{\text{cusped}}(r) = \frac{\rho_0}{\frac{r}{r_s} \left(1 + \frac{r}{r_s}\right)^2}, \quad (6)$$

where ρ_0 is the overall normalisation and r_s the scale radius. The parameters ρ_0 and r_s determining the shape of the profile as well as the halo virial mass M_{vir} are found by solving the following system

of 3 equations:

$$M_{\text{vir}} = \int_0^{R_{\text{vir}}} \rho_{\text{cusped}}(r) d^3\vec{r} \quad (7)$$

$$M_{\text{vir}} = \frac{4\pi}{3} \rho_{200} \times R_{\text{vir}}^3 \quad (8)$$

$$C_{\text{vir}}(M_{\text{vir}}, z) = \frac{c_0}{1+z} \times \left(\frac{M_{\text{vir}}}{10^{14} h^{-1} M_{\odot}} \right)^{\alpha}, \quad (9)$$

where R_{vir} is the halo virial radius. The virial radius is computed given the virial mass M_{vir} and is defined as the radius within which the mean density equals ρ_{200} ($\rho_{200} = 200 \times \rho_c$, where ρ_c is the critical density of the universe ¹).

Eq. 9 relates the concentration parameter C_{vir} to the virial mass. The concentration parameter is defined as the ratio between the virial radius and the scale radius R_{vir}/r_s in the case of a NFW profile. The relation between C_{vir} and M_{vir} is not well-known and was studied in various simulations of structure formation. Eq. 9 is used following the halo concentration fit of (Dolag et al. 2004) which is in good agreement with most of N-body simulations proposed in the literature (see (Bullock et al. 2001) and (5) as examples). In Eq. 9, z denotes the redshift and h the present day normalized Hubble expansion rate. c_0 and α are the parameters of the halo concentration fit and depend on the cosmological scenario ($c_0 = 9.6$ and $\alpha = -0.1$ in a Λ CDM cosmology).

The CMA dSph galaxy is located close to the Galactic disk and suffers from strong tidal disruptions. A reasonably good estimator of its total dark halo mass is then the mass enclosed inside its tidal radius rather than its virial mass. The tidal radius of the CMA dwarf galaxy is calculated via the Roche criterion:

$$\frac{M_{\text{dSph}}(r_t)}{r_t^3} = \frac{M_{\text{MW}}(d - r_t)}{(d - r_t)^3}, \quad (10)$$

where d is the distance of CMA to the center of the MW. $M_{\text{MW}}(r)$ denotes the mass of the MW galaxy enclosed in a sphere of radius r . A NFW profile for the MW halo is considered with a concentration parameter equal to 10 and a virial mass of $10^{12} M_{\odot}$. The total mass of the dSph galaxy is computed by iterative tidal stripping, inserting first M_{vir} in Eq. 10 and computing successively the total halo mass (using Eq. 7) and the tidal radius (using Eq. 10), until the convergence of the procedure is reached. The question is now whether or not tidal forces significantly remodel the internal structure of tidally affected dSph. Discrepant results have been reported in the literature regarding this question (Reed et al.; Stoehr et al. 2002). Here, it is assumed that tidal forces do not affect the inner part of the density profile so that the initial halo structural parameters are kept constant during the stripping procedure. The remaining mass is typically found to be an order of magnitude lower than the virial mass.

The astrophysical term f^{AP} can then be computed as a function of the halo mass by performing the line-of-sight integration of the CMA dSph squared mass density, according to Eq. 5. Table 2

¹<http://pdg.lbl.gov>

shows the obtained NFW structural parameters for three dark matter halos with different virial masses. The integral of the squared mass density increases with the halo mass and the f^{AP} value for a dwarf galaxy of mass $10^8 M_\odot$ located at an heliocentric distance of 8 kpc is found to be in the right order of magnitude ($f^{\text{AP}} \sim 10^{25} \text{ GeV}^2 \text{ cm}^{-5}$) compared to (6).

M_{vir} (M_\odot)	ρ_0 ($10^8 M_\odot \text{ kpc}^{-3}$)	r_s (kpc)	r_t (kpc)	$M(r \leq r_t)$ (M_\odot)	f^{AP} ($10^{24} \text{ GeV}^2 \text{ cm}^{-5}$)
10^6	4.7	0.04	0.28	3.9×10^5	0.24
10^8	1.3	0.28	1.17	3.1×10^7	2.2
10^{10}	0.39	2.08	4.15	1.9×10^9	12

Table 2: Structural parameters of NFW dark matter halos and associated f^{AP} values derived with the procedure described in the text, for three different virial masses.

4.2. Halo independent constraints on the annihilation signal

Using the upper limit γ map on the number of γ -events derived with the γ candidate map and the normalized background map (see Sec.III-B for details), upper limits on the value of $\langle\sigma v\rangle \times f^{\text{AP}}$ can be derived (Eq. 2, Eq. 3, Eq. 4) for various neutralino masses. As an example, Fig. 2(a) shows a sky map of the 95% C.L upper limit values on $\langle\sigma v\rangle \times f^{\text{AP}}$, computed within a pMSSM scenario for a 1 TeV higgsino-like neutralino annihilating in pairs of W and Z gauge bosons. The sensitivity is better toward the center of the FoV, because the H.E.S.S. acceptance decreases on the edges of the camera. H.E.S.S. is sensitive to $\langle\sigma v\rangle \times f^{\text{AP}}$ values of the order of $10^2 \text{ GeV}^2 \text{ cm}^{-2} \text{ s}^{-1}$. Since the core of the CMa dSph can be anywhere in the FoV, one obtains a distribution of the $\langle\sigma v\rangle \times f^{\text{AP}}$ upper limits over the FoV. As shown by Fig. 2(b), this distribution is well fitted by a Gaussian curve. The mean value can be taken as the $\langle\sigma v\rangle \times f^{\text{AP}}$ 95% C.L upper limit reference value and the corresponding 1σ error bar reflects the uncertainties associated to it.

Using this procedure, an exclusion curve in the plane ($\langle\sigma v\rangle \times f^{\text{AP}}, m_{\text{DM}}$) can be derived. The corresponding curve is shown on Fig. 3(a). The grey shaded areas represent the 1σ uncertainties associated with the 1σ error bars on the $\langle\sigma v\rangle \times f^{\text{AP}}$ 95% upper limit.

4.3. Sensitivity to the CMa mass

As the f^{AP} factor is related to the CMa halo mass (see Sec IV.A), an upper limit on the total CMa mass can be obtained using the previously derived exclusion curve on the $\langle\sigma v\rangle \times f^{\text{AP}}$ quantity and assuming a fixed value for the annihilation cross-section. WIMPs velocity-weighted annihilation cross-sections are expected to be of the order of weak-scale interaction cross-sections. Exclusion curves in the plane ($M_{\text{CMa}}^{95\% \text{C.L}}, m_{\text{DM}}$) are then plotted for different annihilation cross-sections within

pMSSM scenarios, using the parametrization of (2) for the γ -ray annihilation spectrum. The corresponding curves are shown on Fig. 3(b). The grey shaded areas represent the 1σ uncertainties associated with the 1σ error bars on the $\langle\sigma v\rangle \times f^{\text{AP}}$ 95% upper limit, as described in the previous section. Annihilation cross-sections larger than $10^{-24} \text{ cm}^3 \text{ s}^{-1}$ are considered here. Lower cross-sections would have been too small to constrain the CMa dSph mass, e.g. the excluded masses would have been of the order of a MW-sized galaxy for typical velocity-weighted annihilation cross-section of $3 \times 10^{-26} \text{ cm}^3 \text{ s}^{-1}$.

4.4. Sensitivity to the annihilation cross-section of WIMP candidates

In this part, the CMa total mass is fixed to be $3 \times 10^8 M_\odot$ and the corresponding value of the astrophysical contribution f^{AP} in the expected γ -ray flux is computed following the procedure described in Sec IV.A. Table 3 compares the value of the CMa dSph and Sgr dSph structural parameters ² assuming a NFW profile. The contribution of the astrophysical term f^{AP} is larger for the CMa dSph than for the Sgr dSph because CMa is closer to the sun. Limits on the velocity-weighted annihilation cross-section $\langle\sigma v\rangle^{95\% \text{C.L}}$ can then be derived as a function of the DM particle mass. Limits are computed in the framework of SUSY and KK models.

	Heliocentric distance (kpc)	ρ_0 ($10^8 M_\odot \text{ kpc}^{-3}$)	r_s (kpc)	f^{AP} ($10^{24} \text{ GeV}^2 \text{ cm}^{-5}$)
CMa	8	1.1	0.55	5.9
Sgr	24	1.4	0.62	2.2

Table 3: Comparison table of the NFW structural parameters of the CMa and Sgr dSph, with their associated f^{AP} values, assuming for both a total mass of $3 \times 10^8 M_\odot$.

The SUSY parameters are computed with the micrOMEGAs v1.37 software package (Belanger et al. 2004). Phenomenological MSSM scenarios have been considered. They are characterized by 7 independent parameters: the higgsino mass parameter μ , the common sfermions scalar mass m_0 , the Higgs fields vacuum expectation value ratio $\tan\beta$, the gaugino mass M_2 , the trilinear couplings A_t and A_b and the CP-odd Higgs mass M_A . Table 4 summarizes the region of the pMSSM parameter space scanned to generate the models. Fig. 4(a) shows the H.E.S.S. exclusion limits on the velocity weighted cross-section. The black points illustrate the computed pMSSM scenarios and the red points represent those satisfying the WMAP+SDSS constraints on the CDM relic density $\Omega_{\text{CDM}} h^2$ (Tegmark et al. 2006). $\Omega_{\text{CDM}} h^2$ is allowed to range between 0.09 and 0.11. The H.E.S.S. observa-

²The NFW structural parameter for the Sgr dSph galaxy were estimated in (6) using the velocity dispersion measurements of the Draco dSph galaxy whereas those of the CMa dSph are derived using numerical simulation results (see Sec IV.A)

tions of the CMa dSph allows to exclude velocity weighted cross-sections of the order of $5 \times 10^{-24} \text{ cm}^3 \text{ s}^{-1}$, comparable with those derived for the Sgr dSph modelled with a cusped NFW profile. The limits obtained are an order of magnitude larger than the velocity-weighted annihilation cross sections of higgsino-like neutralinos.

In the case of KK scenarios, predictions for the velocity-weighted cross-section are computed with

pMSSM parameters
$100\text{GeV} \leq \mu \leq 30\text{TeV}$
$100\text{GeV} \leq m_0 \leq 1\text{TeV}$
$1.2 \leq \tan\beta \leq 60$
$10\text{GeV} \leq M_2 \leq 50\text{TeV}$
$-3\text{TeV} \leq A_{t,b} \leq 3\text{TeV}$
$50\text{GeV} \leq M_A \leq 10\text{TeV}$

Table 4: Region of the pMSSM parameter space scanned to generate the models. A set of free parameters in the considered range is associated to a pMSSM model.

the formula given in (Baltz and Hooper 2005). The expression of $\langle\sigma v\rangle$ is inversely proportional to the squared mass of the lightest Kaluza-Klein (LKP) particle, namely the $B^{(1)}$ particle. Considered KK models that reproduce the CDM relic measured by WMAP and SDSS require a LKP mass ranging from 0.7 TeV to 1 TeV. Fig. 4(b) shows the H.E.S.S. limits obtained within these models. The H.E.S.S. observations do not constrain the KK velocity weighted cross-section.

5. Conclusions

The CMa overdensity is the subject of many debates over whether it is a dwarf galaxy or the warp and flare of the Galactic outer disk. Considering the first scenario, its relative proximity makes it potentially the best region for searches of a DM annihilation signal. However, the lack of observational data prevents the precise modelling of its density profile. Assuming a NFW profile and a mass content of $3 \times 10^8 M_\odot$ within its tidal radius, typical of dwarf galaxies, H.E.S.S. is close to exclude a few pMSSM scenarios with higgsino-like neutralinos, but does not reach the necessary sensitivity to test models compatible with the WMAP+SDSS constraint on the CDM relic density. In the case of DM made of $B^{(1)}$ particle from KK models with extra dimensions, no constraints are obtained.

The support of the Namibian authorities and of the University of Namibia in facilitating the construction and operation of H.E.S.S. is gratefully acknowledged, as is the support by the German Ministry for Education and Research (BMBF), the Max Planck Society, the French Ministry for

Research, the CNRS-IN2P3 and the Astroparticle Interdisciplinary Programme of the CNRS, the U.K. Particle Physics and Astronomy Research Council (PPARC), the IPNP of the Charles University, the Polish Ministry of Science and Higher Education, the South African Department of Science and Technology and National Research Foundation, and by the University of Namibia. We appreciate the excellent work of the technical support staff in Berlin, Durham, Hamburg, Heidelberg, Palaiseau, Paris, Saclay, and in Namibia in the construction and operation of the equipment.

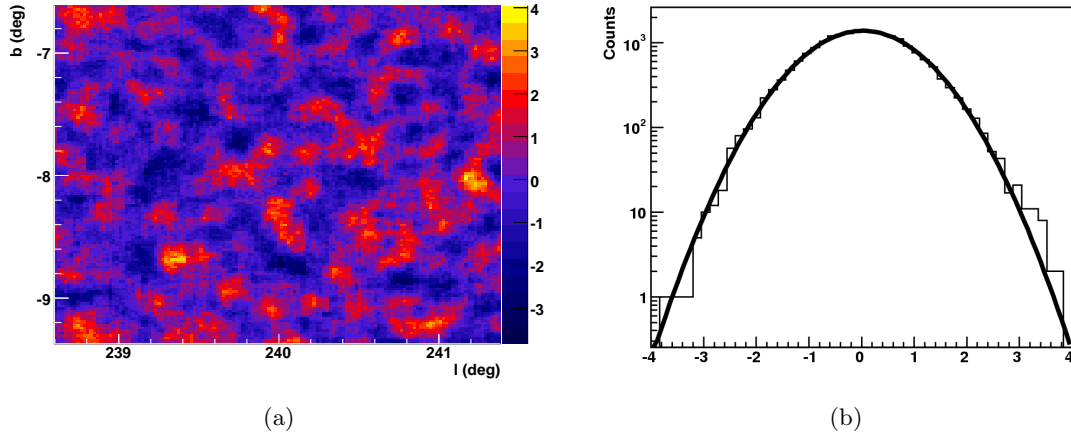


Fig. 1.— (a) Significance map corresponding to the excess map computed in the analysis (see text), calculated according to the Li & Ma method (Li and Ma 1983). (b) Significance distribution derived from the significance map. The solid line shows the Gaussian fit. The mean value is 0.01 ± 0.004 and the corresponding variance is 1.000 ± 0.005 .

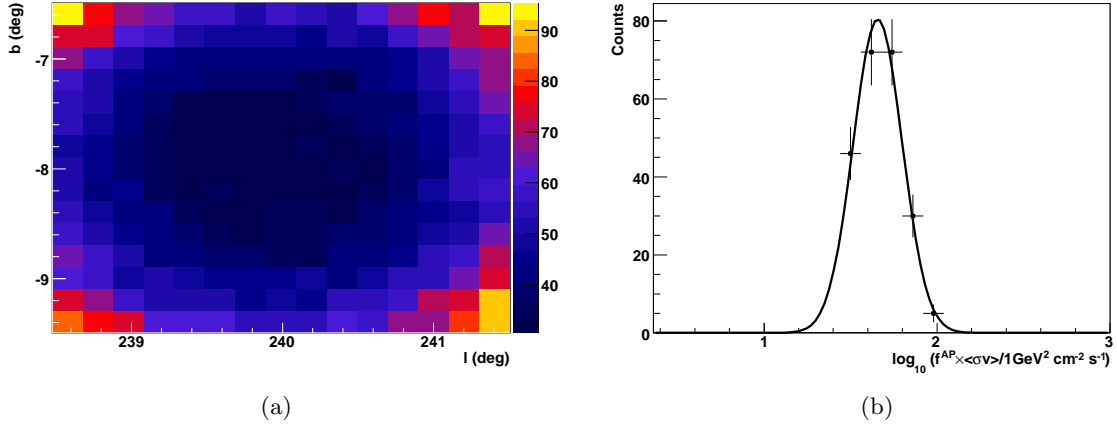


Fig. 2.— (a) 95% C.L. upper limit map on the value of $\langle\sigma v\rangle \times f^{\text{AP}}$ derived for a 1 TeV neutralino (see text). (b) Distribution of the 95% C.L. $\langle\sigma v\rangle \times f^{\text{AP}}$ upper limits logarithm derived with the upper limit map from (a). The solid line shows the Gaussian fit. The mean value is 1.66 ± 0.01 and the corresponding variance is 0.14 ± 0.01 .

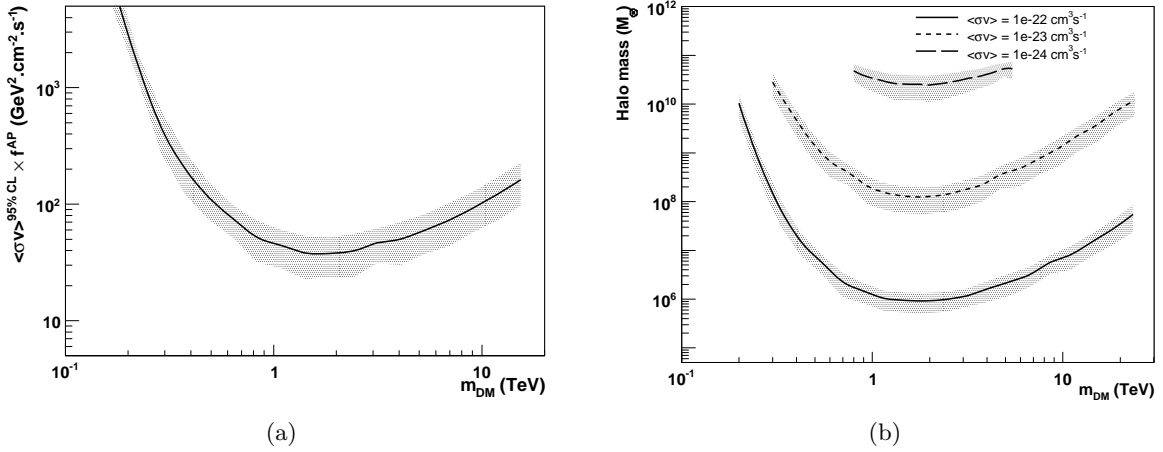


Fig. 3.— (a) Upper limits at 95% CL on the value of $\langle\sigma v\rangle \times f^{\text{AP}}$ as a function of the DM particle mass in the framework of pMSSM scenarios. (b) Upper limits at 95% CL on the CMa total mass versus the DM particle mass for different annihilation cross-sections in pMSSM scenarios. The shaded area represents the error bars issued from the 1σ error on the $\langle\sigma v\rangle \times f^{\text{AP}}$ distribution Gaussian fits (see text for details).

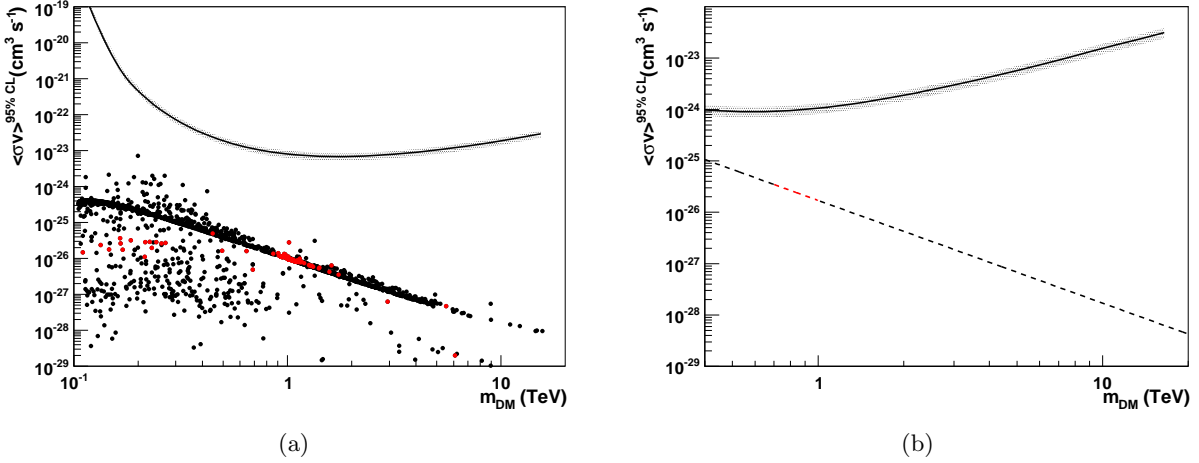


Fig. 4.— Upper limits at 95% CL on the velocity weighted cross-section as a function the DM particle mass in the case of pMSSM (a) and KK (b) scenarios, for an assumed CMa total mass of $3 \times 10^8 M_{\odot}$. The shaded area represents the 1σ error bars on $\langle\sigma v\rangle^{95\% \text{C.L}}$ (see text for details). (a) The pMSSM models are represented by black points, and those giving a CDM relic density in agreement with the measured WMAP+SDSS value are illustrated by red points. (b) The KK models are represented by the black dashed line, and those verifying the WMAP+SDSS constraint on $\Omega_{\text{CDM}}h^2$ are labelled in red.

REFERENCES

- Aharonian F., et al. 2004, *A&A*, 425, L13
- Aharonian F., et al. 2005, *A&A*, 430, 865
- Aharonian F., et al. 2006a, *Science*, 314, 1424
- Aharonian F., et al. 2006b, *A&A*, 457, 899
- Aharonian F., et al. 2006c, *Phys. Rev. Lett.*, 97, 221102
- Aharonian F., et al. 2008, *Astropart. Phys.*, 29, 55
- Albert J., et al. 2007, preprint (astro-ph/07112574)
- Baltz E., Hooper D. 2005, *JCAP*, 0507, 001
- Belanger G., Boudjema F., Pukhov A., Semenov A. 2004, preprint (hep-ph/0405253)
- Bellazinni M., et al. 2004, *MNRAS*, 354, 1263
- Berge D., Funk S., Hinton J. 2007, *A&A*, 466, 1219
- Bergström L., Ullio P., Buckley J. 1998, *Astropart. Phys.*, 9, 137
- Bergström L., Bringmann T., Eriksson M., Gustafsson M. 2005a, *Phys. Rev. Lett.*, 94, 131301
- Bergström L., Bringmann T., Eriksson M., Gustafsson M. 2005b, *Phys. Rev. Lett.*, 95, 241301
- Bertone G., Hooper D., Silk J. 2005, *Phys. Rept.*, 405, 279
- Bullock J., et al. 2001, *MNRAS*, 321, 559
- Colafrancesco S., Profumo S., Ullio P. 2007, *Phys. Rev.*, D75, 023513
- Dekel A., Silk J. 1986, *ApJ*, 303, 39
- Dolag K., et al. 2004, *A&A*, 416, 853
- Eke V.R., Navarro J.F., Steinmetz M. 2001, *ApJ*, 554, 114
- Evans N.W., Ferrer F., Sarkar S. 2004, *Phys. Rev.*, D69, 123501
- Feldman G., Cousins R. 1998, *Phys. Rev.*, D57, 3873
- Hofmann W., et al. 2003, in *Proc. of the 28th ICRC (Tsubuka)*, Vol.1, p.2811
- de Jong J. T. A., et al. 2007, *ApJ*, 662, 259D
- Jungman G., Kamionkowski K., Griest K. (1996), *Phys. Rept.*, 276, 195

- Li T., Ma Y. 1983, ApJ, 272, 317
- Martinez-Delgado D., et al. 2004, preprint (astro-ph/0410611)
- Martin N.F., et al. 2004, MNRAS, 348, 12
- Mateo M. 1998, Annu. Rev. Astron. Astrophys., 36, 435
- Momany Y., et al. 2006, A&A, 451, 515
- Navarro J., Frenk C., White S. 1997, ApJ, 490, 493
- de Naurois M., et al. 2003, in Proc. of the 28th ICRC (Tsubuka), Vol.5, p2907
- Reed D., et al. 2005, MNRAS, 357, 82
- Rowell G.P. 2003, A&A, 410, 389
- Servant G., Tait T. 2003, Nucl. Phys., B650, 391
- Sjöstrand T., Lönnblad L., Mrenna S., Skands P. 2003, PYTHIA 6.3, preprint (hep-ph/0308153)
- Stoehr F., et al. 2002, MNRAS, 335, L84
- Tegmark M., et al. (2006, Phys. Rev., D74, 123507
- Walker M.G., et al. 2007, ApJ, 667, L53
- Wood M., et al. 2007, preprint (astro-ph/08011708)